ROYAL SOCIETY OF CHEMISTRY

PAPER

Check for updates

Hydroxyl radical-initiated degradation kinetics of organic pollutants in surfactant-rich environments

Carole Abdel Nour, Stéphanie Rossignol, [ID] * Boulos Samia, [ID] Maria Bou Saad, [ID] Ndeye Khoyane Dieng, Stéphanie Lebarillier, Laurence Asia, Anne Monod and Pascal Wong-Wah-Chung

Surfactant-rich aqueous media are common in natural environments. The sea surface microlayer and sea spray droplets are good examples and are also frequently markedly enriched in organic pollutants. This study focuses on the degradation kinetics of organic pollutants initiated by the hydroxyl radical in such surfactant-rich environments. The apparent second-order rate constants of the reaction of the hydroxyl radical with two model pollutants, carbamazepine and phenanthrene, were determined in the presence of sodium dodecyl sulfate or rhamnolipids at concentrations below and above their critical micelle concentration (CMC). The results show that the apparent rate constant remains unaffected below the CMC, unless additional reactive processes are induced. From the results obtained above the CMC, second-order rate constants were derived for the reaction of the hydroxyl radical with the pollutant trapped in the surfactant micelles. A rather similar decrease of about a factor of 3 in comparison to pre-micellar conditions was observed for all three experimental conditions tested. This work appears to provide a suitable foundation for evaluating the impact of such surfactant-rich environments on the half-lives and fates of organic pollutants and a preliminary indication of how reaction kinetics may be modified in various organized surfactant structures.

Environmental significance

Photo-induced processes represent a significant pathway for the degradation of most organic pollutants. Studying the kinetics of these processes is of paramount importance for the evaluation of the lifetime of these pollutants in aqueous surface and atmospheric compartments. Here, we expanded the existing knowledge on this subject by investigating the degradation kinetics of pollutants in surfactant-rich aqueous media. Indeed, organic pollutants are known to be enriched in such media, *e.g.*, in the sea surface microlayer. This work shows that surfactants can increase the pollutants' lifetime against hydroxyl radical attack through both radical quenching and micelle trapping. It provides a quantitative assessment of the decrease in reaction rate constants, enabling this modified kinetics to be taken into account in models.

1. Introduction

Assessing the fate of pollutants in the environment is a crucial task in determining their impact on ecosystems and human health. The pollutant's half-life and the structures of its degradation products are essential data in this context, contributing to accurate risk assessment by evaluating the pollutant's persistence and the potential adverse effects resulting from its transformation.

However, the chemical processes involved may depend on both the pollutant and the environment, introducing a complexity that is often underestimated in risk assessment. An example of this is the observed slower degradation rate of pesticides by gas phase hydroxyl radicals sorbed onto/into atmospheric particles compared to gas phase pesticides. The

Aix Marseille Univ., CNRS, LCE, Marseille, France. E-mail: stephanie.rossignol@univ-amu.fr

difference is significant as this slower rate would explain the unexpected long-range atmospheric transport of some of these compounds.[1–4] Another example is the inhibiting or amplifying effect of different organic coatings on the kinetics of the heterogeneous reaction of polycyclic aromatic hydrocarbons (PAHs) with ozone at the air–water interface.[5,6]

In natural surface waters, the fate of organic pollutants is strongly linked to light-initiated degradation processes. This photochemistry is most often studied in the homogeneous dilute phase. Kinetic rate constants are inferred from laboratory photodegradation experiments and are then used to predict the pollutant half-lives in a given body of water, taking into account variations in light flux and concentrations of organic and inorganic matter.[7–9] An interesting application of this is the recent study by Rosso and Vione[10] in which they modelled half-lives of emerging pollutants in the context of evaporative surface water concentration in arid and semi-arid environments predicting modifications in the involvement of the different

This journal is © The Royal Society of Chemistry 2025

Environ. Sci.: Processes Impacts, 2025, **27**, 3119–3131 | 3119

degradation pathways (direct photolysis, triplet sensitized reactions, *etc.*). This highly instructive study nevertheless assumes that reaction rate constants remain unchanged regardless of the concentration factor. If this assumption seems justified in the range examined, *i.e.*, a water depth decreasing to one meter, it would appear to require reassessment when approaching a depth of zero meters.

The presence of organic compounds with surface-active properties (of biogenic or anthropogenic origin) could, for instance, lead to the formation of micelles or related organized structures (monolayers, vesicles, *etc.*) in which the organic pollutants can partition, due to hydrophobic interactions.[11–20] This could potentially modify reaction kinetics and/or preferential pathways.[18,21–23] This type of organic-rich medium, with a significant fraction of surface-active compounds, is not uncommon in the environment. The sea surface microlayer (SML) for instance is enriched in compounds with surface-active properties.[24–26] These biogenic surface-active compounds, such as carbohydrates, proteins, and lipids, arise from the water column through adsorption at the surface of air bubbles produced mainly by breaking waves.[27] Visible slicks (with at least a monolayer of organic matter at the air–water interface) are stable for wind speeds of up to 4 m s^{-1} and a SML can exist up to wind speeds of 6–10 m s^{-1}. The SML is thus almost ubiquitous.[28] Sea spray droplets, emitted into the atmosphere when the plumes of air bubbles generated by breaking waves burst at the ocean surface, are also enriched in organic matter, including compounds with surface-active properties, compared to bulk sea water[29–32] and individual concentrations can increase upon droplet evaporation and the formation of sea spray aerosol (SSA).

It is also important to note that concentrations of organic pollutants are likely to be higher in these organic-rich media than in the more studied diluted phase. Rosso and Vione[10] logically supposed increased organic pollutants concentrations in evaporative waters. Organic pollutants, especially the most hydrophobic ones (PCBs, aliphatic and aromatic hydrocarbons, PFASs, *etc.*), are found to be enriched in the SML[33–38] with enrichment factors compared to the underlying water reaching up to 950 (value for anthracene in a harbor[38]), and can include anthropogenic surfactants.[39,40] Moreover, it has been shown that these pollutants can be transferred in SSA, with enrichment factors compared to bulk sea water increasing as the SSA size decreases, particularly in the submicron range.[37,38,41,42] In these surfactant-rich environments, organic pollutants can partition into micelles (or related structures) and/or into surfactant monolayers or multilayers at the water–air interface.[43–45] Kinetic and photochemical pathways may then differ significantly from those observed in the diluted phase.[22,46]

The aim of this work is thus to investigate the photochemical fate of organic pollutants in surfactant-rich natural environments, such as the SML or evaporative water droplets from sea spray. This study focuses on the degradation kinetics of two pollutants with significantly different water solubilities and octanol–water partition coefficients (K_{ow}), carbamazepine and phenanthrene (log K_{ow} of 2.45 (ref. 47–49) and 4.46–4.65 (ref. 50 and 51) respectively). Here, we studied hydroxyl radical-initiated degradation in the presence of either sodium dodecyl sulfate (SDS), a well-characterized anionic surfactant that can also be found in the environment, or rhamnolipids (RLs), a biosurfactant that may better represent surfactants of biogenic origin encountered in environmental samples. Structures of pollutants and surfactants are presented in Fig. 1. The apparent rate constants of reaction between the pollutant and hydroxyl radicals were determined following the competition
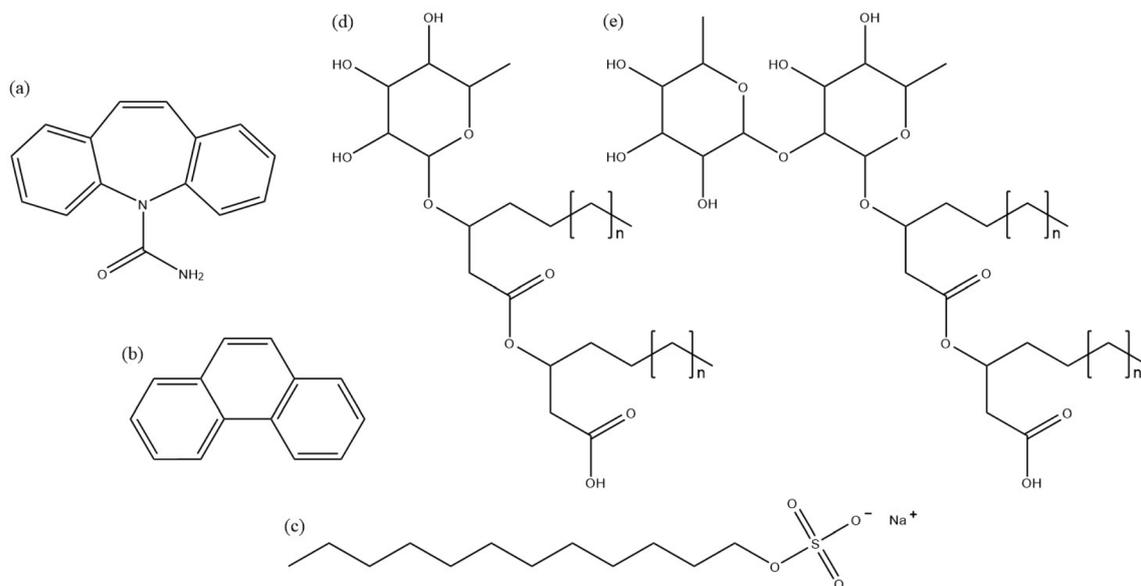

Fig. 1 Structures of (a) carbamazepine (CBZ), (b) phenanthrene (Phe), (c) sodium dodecyl sulfate (SDS), (d) mono-rhamnolipids, and (e) di-rhamnolipids (RLs). The chain length ($n + 6$) of the commercial mixture of mono- and di-rhamnolipids used in this study is unknown but was assumed to be ten carbon atoms ($n = 4$) for micellar volume calculations (see the SI for details).

3120 | *Environ. Sci.: Processes Impacts*, 2025, **27**, 3119–3131

This journal is © The Royal Society of Chemistry 2025

kinetics method, using the reaction of terephthalic acid (TPA) with hydroxyl radicals as the reference.

2. Methods

2.1. Chemicals

Carbamazepine (CBZ, 99% purity), phenanthrene (Phe, 99.5% purity), terephthalic acid (TPA, 98% purity), fluoranthene (Fluo, 98% purity), sodium dodecyl sulfate (SDS, >99% purity), rhamnolipids biosurfactants from *Pseudomonas aeruginosa* (RLs, 90% purity), acetonitrile (HPLC grade, ≥99.9% purity), hexane (≥99.9% purity), dichloromethane (≥99.8% purity, amylene as the stabilizer) and dimethylformamide (≥99% purity) were purchased from Sigma-Aldrich (St-Louis, USA) and used without further purification. Non stabilized hydrogen peroxide (H_2O_2, 30 wt% solution in water) was provided by Thermo Fisher Scientific. Potassium hydroxide pellets (KOH, >85%) were purchased from Carlo Erba Reagents (Milano, Italy) and a stock solution was prepared every month at 0.1 M. Stock solutions of Fluo were prepared in hexane at a concentration of 50 mg L^{-1} in a 100 mL amber glass bottle and stored at 4 °C. All aqueous solutions were prepared with ultrapure water (Merck, Direct-Q® 5 UV, 18.2 MΩ cm).

2.2. Determination of the critical micelle concentration of SDS and RLs

The critical micelle concentration (CMC) of SDS was determined using conductivity measurements at room temperature. The conductivity ($\mu S\ cm^{-1}$) of a series of SDS solutions with various concentrations was measured using a conductivity meter Multi 340i and a measuring cell TetraCon 325 from WTW®. Conductivity was plotted as a function of surfactant concentration. Since free surfactant molecules have a different molar conductivity compared to micellar surfactant molecules, the CMC is identified as the point on the plot where the slope changes. The CMC of RLs was determined using the pendant drop technique. The surface tension (ST) of RL solutions was measured with a drop shape analyzer DSA-30 from Krüss. The shape of the drop hanging from a needle is determined by the balance of forces which includes the surface tension of the liquid. The surface tension can be related to the drop shape by the Young–Laplace equation. The accuracy of the measurements is ±0.1 mN m^{-1}. Prior to each experiment, the instrument was calibrated by measuring the surface tension of pure water. The CMC is determined by measuring the ST of a series of RL solutions with different concentrations. Above the CMC, ST becomes independent of surfactant concentration. ST was plotted as a function of the decimal logarithm of the surfactant concentration. The CMC is identified as the point of intersection between the regression straight line of the linearly dependent region and the straight line passing through the plateau.

2.3. CBZ degradation experiments

The CBZ photodegradation experiments were carried out in a photoreactor equipped with a xenon arc lamp (300 W – LOT Quantum Design, France). The lamp outlet is equipped with a water filter that eliminates infrared radiation ($\lambda > 800$ nm) and helps reduce the thermal load. The horizontal beam is deflected at a 90° angle by a dichroic mirror before passing through an atmospheric attenuation filter that removes ultraviolet radiation below 290 nm before reaching the water surface in the reactor. The resulting lamp spectrum is provided in the SI (Fig. S1). The reactor has a volume of approximately 100 mL, and the experiments took place in 50 mL of the reaction mixture. Throughout all experiments, the reactor was hermetically closed with a cap with a quartz window and was equipped with a double wall that allowed water circulation and regulation of the temperature at (20 ± 1) °C. Homogeneity was ensured by magnetic stirring. Sampling was performed through a side sampling port.

Stock solutions of CBZ and TPA were prepared at 1.6×10^{-4} M and 4.8×10^{-5} M respectively using ultrapure water (Merck, Direct-Q® 5 UV, 18.2 MΩ cm) and stored in the dark at 4 °C. Working solutions were prepared before each experiment by dilution of stock solutions in ultrapure water to concentrations of 2×10^{-5} M for each reagent and the pH was adjusted to 8.2 using a 0.1 M KOH solution. This pH was chosen because it is representative of marine environments and because it implies the predominance of the doubly deprotonated form of TPA ($pK_{aTPA} = 3.51$ and 4.82), which strongly limits the partitioning of TPA in surfactant micelles. Hydroxyl radicals were produced by H_2O_2 photolysis. The concentrations of H_2O_2 and surfactant (SDS or RLs) added in each experiment were estimated to achieve a degradation of about 70–80% of CBZ within 4 hours of irradiation, using a kinetic model based on the known reaction rate constants of CBZ, TPA and SDS towards ˙OH radicals. A summary of the initial conditions of all the experiments performed with CBZ is provided in the SI (Tables S1 and S2). Aliquots of the reaction mixture were taken from the reactor for CBZ and TPA quantification right before the irradiation was turned on and after 30, 60, 120, 180 and 240 minutes.

2.4. Phe degradation experiments

The Phe photodegradation experiments were carried out using an irradiation chamber equipped with 3 UV fluorescent tubes (CLEO Compact S 25W from iSOLde). The spectral irradiance at the center of the chamber is provided in the SI (Fig. S2). The chamber is equipped with a ventilation system to maintain a constant temperature of (25 ± 2) °C inside the box throughout the experiments.

The reactor was a glass crystallizer on which a quartz plate was sealed with a Teflon gasket prior each experiment. The crystallizer was filled with 200 mL of the reaction mixture, thereby ensuring that the headspace volume was minimized to limit the volatilization of Phe. Homogeneity was ensured by magnetic stirring.

A stock solution of both Phe and TPA at concentrations of 5.6×10^{-6} and 3×10^{-5} M respectively was prepared in one liter of ultrapure water every two weeks. This solution was left under magnetic stirring for 2 days in the dark at room temperature to maximize the solubilization of phenanthrene. Prior to each experiment, 200 mL of the stock solution were filtered into the reactor through a hydrophilic PTFE filter (0.22 μm Clarify-PTFE

This journal is © The Royal Society of Chemistry 2025

Environ. Sci.: Processes Impacts, 2025, 27, 3119–3131 | 3121

(hydrophilic) syringe filters from Phenomenex). The pH was then adjusted to 8.2 using a 0.1 M KOH solution. The concentration of H_2O_2 and surfactant (SDS or RLs) added in each experiment was estimated to achieve a degradation of about 70–80% of Phe within 4 hours of irradiation, using a kinetic model based on the known reaction rate constants of Phe, TPA and SDS towards $^{\bullet}$OH radicals. A summary of the initial conditions of all the experiments performed with Phe is provided in the SI (Tables S3 and S4). Aliquots of the reaction mixture were taken from the reactor for Phe and TPA quantification right before the irradiation and after 30, 60, 120, 180 and 240 minutes of exposure.

2.5. Analytical methods

The analyses of CBZ and TPA were carried out by high performance liquid chromatography using a UHPLC PerkinElmer FX 10 equipped with a 330-diode array UV-visible detector (Flexar PDA Plus model) and a 410 automatic injector. The chromatographic separation was carried out on a Brownlee SPP RP-amide column (150 mm × 2.1 mm; 2.7 μm) maintained at 30 °C. The volume of the reaction mixture injected was 10 μL. Analytes were separated with a mixture of acetonitrile/water with 0.1% formic acid at a flow rate of 0.5 mL min^{-1} using the following gradient: from 5% to 50% acetonitrile within 20 min and then back to initial conditions within 5 min. TPA and CBZ were detected at $\lambda = 241$ and 285 nm respectively. Under these conditions, their retention times were 8 and 20 min respectively. The data were processed using Chromera software.

For Phe extraction and concentration (SI-Fig. S3), 5 mL aliquots of the reaction mixture were sampled and Fluo (20 μL of the stock solution), used as an extraction surrogate, was introduced. The aliquots were then extracted 4 times, adding 5 mL of dichloromethane and agitating on a rotary agitator for 7 min at each cycle. The combined 20 mL of dichloromethane extract was then evaporated to 1 mL, 100 μL of dimethylformamide were added and the remaining dichloromethane was evaporated. 900 μL of acetonitrile were then added and the 1 mL solutions were filtered onto a 0.22 μm PTFE filter before chromatographic analysis. In the presence of SDS in the reaction mixture, 200 mg of KCl was introduced after Fluo addition and prior to dichloromethane extraction to precipitate SDS and avoid excessive foaming. The overall Phe recovery was estimated to be $(95 \pm 4)\%$ (SI-Table S5).

The analysis of Phe and Fluo was carried out using a UHPLC PerkinElmer FX6a coupled to an Atlus A-30 fluorescence detector. An Agilent Chromsep pursuit 5PAH column (250 mm × 4.6 mm; 5 μm) equipped with a precolumn CP 28151 was used and maintained at 30 °C. The injected volume was 10 μL. Analytes were separated with a mixture of acetonitrile/water (80 : 20, v/v) with 0.1% formic acid at a flow rate of 1.2 mL min^{-1} in isocratic elution mode. Detection of Phe and Fluo were performed at $\lambda_{ex}/\lambda_{em}$ of 248/375 and 280/462 nm, respectively. The data were processed using software Waters Empower®.

2.6. Kinetics data treatment

Apparent second order reaction rate constants between the pollutant and hydroxyl radicals, $k_{app(pollutant,HO^{\bullet})}$, were determined following the competition kinetics method.[52] TPA was

selected as the reference compound.[53,54] Since TPA is doubly deprotonated at pH 8.2 ($pK_{aTPA} = 3.51$ and 4.82), its partitioning into the negatively charged micelles of surfactant is considered negligible. Its reaction rate constant with hydroxyl radicals, $k_{(TPA,HO^{\bullet})}$, has been reported to be $(4.4 \pm 0.1) \times 10^9$ M^{-1} s^{-1}.[54] The apparent second order rate constant for the reaction between the pollutant and hydroxyl radicals, $k_{app(pollutant,HO^{\bullet})}$, was determined using the following equation (see the SI for details):

$$\ln \frac{[\text{pollutant}]_t}{[\text{pollutant}]_0} = \frac{k_{app(pollutant,HO^{\bullet})}}{k_{(TPA,HO^{\bullet})}} \ln \frac{[\text{TPA}]_t}{[\text{TPA}]_0} \quad (1)$$

where $[\text{pollutant}]_0$ and $[\text{TPA}]_0$ are the initial concentrations and $[\text{pollutant}]_t$ and $[\text{TPA}]_t$ are the concentrations remaining in the solution at irradiation time t. The ratio $k_{app(pollutant,HO^{\bullet})}/k_{(TPA,HO^{\bullet})}$ corresponds to the slope of the linear regression obtained by monitoring pollutant and TPA concentrations over time, from which $k_{app(pollutant,HO^{\bullet})}$ was inferred. The uncertainty for each $k_{app(pollutant,HO^{\bullet})}$ value was estimated based on the standard deviation of replicate measurements (SI-Tables S1 to S4) and the uncertainty associated with the $k_{(TPA,HO^{\bullet})}$ value.

2.7. Adaptation of the micellar pseudophase model

The pseudophase model provides a theoretical approach to describe reaction kinetics in heterogeneous systems. In this model,[23,55,56] the total available volume of micelles formed by a given surfactant S (V_{Sm}) is treated as a conventional reaction medium. Here, as the hydroxyl radical is a transient species, this model was adapted (see the SI for details) assuming that the hydroxyl radical is in the aqueous phase and can react either with the pollutant P solubilized in the water phase or with the pollutant entrapped in the micellar pseudophase. The apparent second-order reaction rate constant for the reaction of a pollutant with hydroxyl radicals, $k_{app(pollutant,HO^{\bullet})}$, can then be expressed as a function of the true second-order reaction rate constant for the reaction of hydroxyl radicals with the water-solubilized pollutant, $k_{(w-pollutant,HO^{\bullet})}$, the true second-order reaction rate constant of the reaction of hydroxyl radicals with the pollutant molecules trapped into the micelles of the surfactant, $k_{(Sm-pollutant,HO^{\bullet})}$, the partition coefficient of the pollutant between the surfactant micelles and water, $K_{mw(pollutant,S)}$, and the total micellar volume, V_{Sm} (eqn (2)):

$$k_{app(pollutant,HO^{\bullet})} = \frac{k_{(w-pollutant,HO^{\bullet})} + k_{(Sm-pollutant,HO^{\bullet})} K_{mw(pollutant,S)} V_{Sm}}{1 + K_{mw(pollutant,S)} V_{Sm}}$$

(2)

The experimental values of $k_{app(pollutant,HO^{\bullet})}$ were plotted as a function of V_{Sm} and fitted using eqn (2), allowing the estimation of the three equation parameters $k_{(w-pollutant,HO^{\bullet})}$, $k_{(Sm-pollutant,HO^{\bullet})}$ and $K_{mw(pollutant,S)}$.

3. Results and discussion

3.1. Determination of the critical micelle concentrations

The CMC of SDS in ultrapure water was found to be 2300 mg L^{-1} (≈ 8.0 mM) (SI-Fig. S4 and Table S6). This value is in the range

3122 | Environ. Sci.: Processes Impacts, 2025, 27, 3119–3131

This journal is © The Royal Society of Chemistry 2025

of those reported in the literature, which generally fall in the 7.9–8.3 mM range at 25 °C.[57–60] The presence of CBZ (2×10^{-5} M), H_2O_2 (1 M) and KOH (for pH adjustment at 8.2) induced no significant change, with a mean CMC value of 2192 ± 223 mg L^{-1}. This latter value was used to estimate the total volume of SDS micelles in the framework of the micellar pseudophase model.

RL surfactants used in this study were shown to reduce the surface tension of water from 72 to 32 mN m^{-1} at room temperature. The CMC value of the RL solution in ultrapure water was about 145 mg L^{-1} (SI-Fig. S5). This value has been used to estimate the total volume of RL micelles in the framework of the micellar pseudophase model. The previously reported CMC values range from 1.6 to 400 mg L^{-1}.[61–63] This broad variation in CMC values is likely due to the fact that RLs are produced by different strains under varying production conditions, leading to different proportions of mono- and di-rhamnolipids. The extraction and purification methods used to isolate rhamnolipids from microbial cultures can also affect the purity and composition of the rhamnolipid samples, potentially leading to differences in reported CMC values.

3.2. Degradation kinetics in the presence of SDS

3.2.1. CBZ degradation kinetics. The photochemical stability of CBZ in ultrapure water at pH 8.2 was validated under our experimental conditions (SI-Fig. S6). In a preliminary series of experiments, slower CBZ degradation rates were observed in the presence of increasing concentrations of SDS for a given initial H_2O_2 concentration (SI-Fig. S7), reflecting the quenching of ·OH radicals by SDS molecules ($k_{(SDS,HO^·)} = 8.2 \times 10^9$ M^{-1} s^{-1} (ref. 64)). Nevertheless, this simple approach suffers from reproducibility issues, which make the determination reaction rate constants unreliable. To address this, the competition kinetics method was used to infer the second order apparent rate constant for the reaction of ·OH radicals with CBZ, $k_{app(CBZ,HO^·)}$, for each experimental condition. Fig. 2(a) shows the results obtained for CBZ in the presence of increasing concentrations of SDS.

The rate constant value obtained in the absence of surfactant, $(7.39 \pm 0.24) \times 10^9$ M^{-1} s^{-1}, is within the range of previously reported values, which vary from 2.05 to 18×10^9 M^{-1} s^{-1}.[65–67] Discrepancies may arise due to temperature and pH dependencies and the determination method employed. The presence of SDS at concentrations below the CMC does not significantly affect the value of the apparent reaction rate constant, indicating that SDS monomers can inhibit the degradation of CBZ but only by acting as a hydroxyl radical quencher. Conversely, above the CMC, a significant decrease in the value of the apparent reaction rate constant is observed. This decrease is not linear and tends to reach a plateau at high SDS concentrations. According to previous studies, the neutral CBZ molecules are assumed to partition into the apolar SDS micelle core.[68,69] The total volume of the SDS micelles, V_{SDSm}, was estimated assuming a micellar radius of 1.84 nm and 64 monomers per micelle (ref. 70) (see the SI for details). V_{SDSm} increases linearly with the SDS concentration above the CMC (Fig. S8(a)).
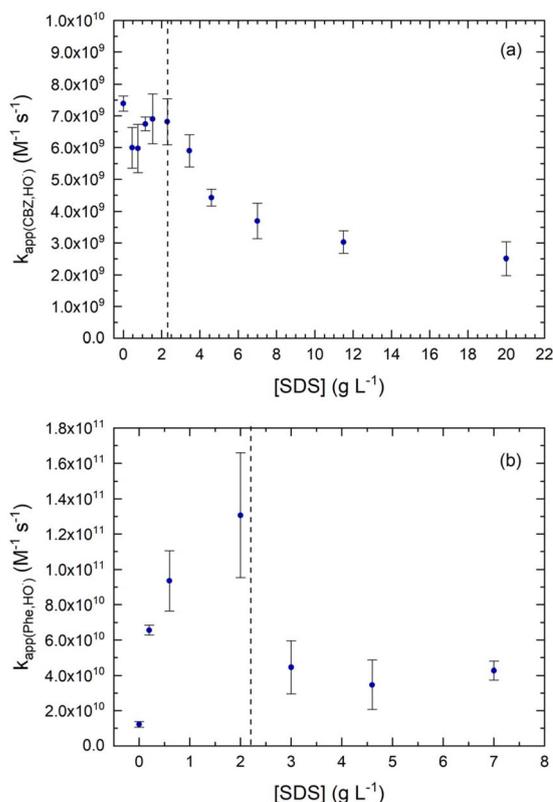

Fig. 2 Apparent second-order rate constant for the reaction of hydroxyl radicals with (a) CBZ and (b) Phe as a function of SDS concentration. Error bars correspond to the uncertainty estimated based on the standard deviation of replicate measurements and the uncertainty associated with the $k_{(TPA,HO^·)}$ value. The vertical dashed line indicates the CMC of SDS.

The experimental values of $k_{app(CBZ,HO^·)}$ were plotted as a function of V_{SDSm} and fitted using eqn (2) (Fig. 3(a)). The resulting estimated values of the three equation parameters $k_{(w-CBZ,HO^·)}$, $k_{(SDSm-CBZ,HO^·)}$ and $K_{mw(CBZ,SDS)}$ were $(7.25 \pm 0.54) \times 10^9$ M^{-1} s^{-1}, $(1.88 \pm 0.42) \times 10^9$ M^{-1} s^{-1} and 489 ± 171, respectively (Table 1). CBZ shielding by SDS micelles thus results in a 74% decrease in the second-order rate constant of its reaction with hydroxyl radicals. This decrease in the reaction rate constant leads to an increase in the half-life of CBZ with respect to its reaction with HO· radicals by a factor of 3.8. The estimated value of log $K_{mw(CBZ,SDS)}$ is 2.69, with an uncertainty range of 2.50 to 2.82. This value is within the range of the published CBZ octanol–water partition coefficient (log $K_{ow,CBZ}$), which varies from 1.51 to 2.77 for calculated values, with a commonly used experimental value of 2.45.[47–49] Using this log $K_{mw(CBZ,SDS)}$ value, the molar fraction of CBZ trapped in SDS micelles was inferred (see the SI for details) and plotted as a function of SDS concentration (Fig. 3(b)). This figure shows that, even for a fairly water-soluble compound such as CBZ, the molar fraction of molecules trapped in SDS micelles rapidly becomes non-negligible above the CMC of SDS, reaching a value of 0.5 at twice the CMC (corresponding to a V_{SDSm} of 2 mL L^{-1}).

This journal is © The Royal Society of Chemistry 2025

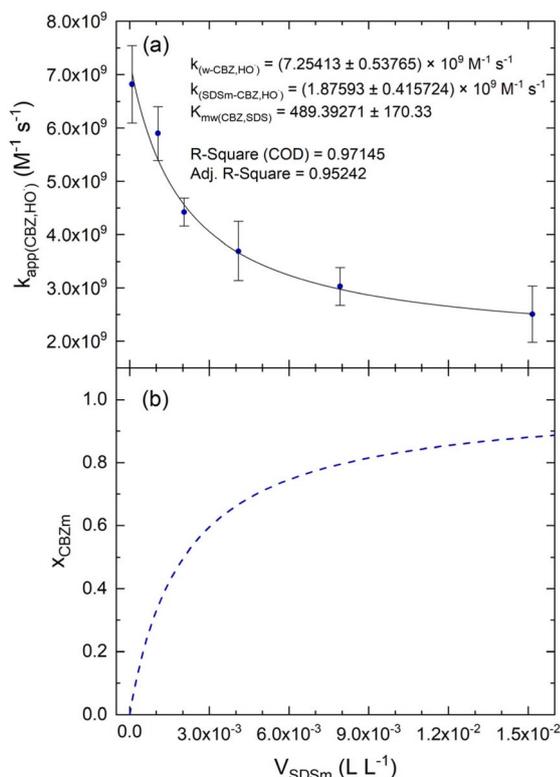*Environ. Sci.: Processes Impacts*, 2025, **27**, 3119–3131 | 3123

Fig. 3 (a) Apparent second-order reaction rate constant measured for the reaction of hydroxyl radicals with CBZ as a function of estimated total SDS micelle volume fitted with eqn (2). (b) Corresponding estimated molar fraction of CBZ trapped into SDS micelles as a function of estimated total SDS micelle volume.

3.2.2. Phe degradation kinetics. The experimental conditions used for Phe degradation experiments were determined so that the direct photolysis as well as the volatilization of Phe can

be considered negligible (SI-Fig. S9). The evolution of the measured apparent rate constant of the reaction between hydroxyl radicals and Phe as a function of SDS concentration is shown in Fig. 2(b). The reaction rate constant value obtained without SDS, $(1.22 \pm 0.16) \times 10^{10}$ M^{-1} s^{-1}, is in good agreement with the lowest previously reported values that range from 1.24×10^{10} to 2.3×10^{10} M^{-1} s^{-1}.[71,72]

In contrast to the results obtained for CBZ, the apparent second-order reaction rate constant for Phe increased with SDS concentration below the CMC and reached a maximum of $(1.31 \pm 0.36) \times 10^{11}$ M^{-1} s^{-1} close to the CMC. This increase causes the rate constant to exceed the classical diffusion-controlled limit value observed for bimolecular reactions in the aqueous phase at ambient temperature, which is around 10^{10} M^{-1} s^{-1}.[73] The diffusion-controlled limit arises from molecular agitation in a medium at a certain temperature, and due to the fact that the reaction cannot occur faster than the rate at which reactive molecules collide. Molecular diffusion depends on the medium properties, including viscosity, the size of the reactants, and temperature. Here, the diffusion limited rate constant was determined to be approximately 8.5×10^9 M^{-1} s^{-1} (see the SI for calculation details). The reaction of Phe with hydroxyl radicals in the absence of surfactant is thus probably limited by diffusion. Since the actual rate constant of the reaction cannot exceed the diffusion rate constant, parallel processes must be involved in the presence of SDS. Enhanced direct photolysis is excluded as Phe stability was validated in the presence of SDS (SI-Fig. S9). This increase in the apparent second-order reaction rate constant corresponds to a decrease in the Phe half-life by a factor of almost 11. Complementary experiments carried out in the presence of RLs instead of SDS at concentrations below the CMC show no significant influence on the apparent rate constant (SI-Fig. S10). This suggests the

Table 1 Second-order rate constants previously reported and those determined in this study for the reaction of CBZ and Phe with hydroxyl radicals, previously reported octanol–water partitioning coefficients and surfactant micelles–water partitioning coefficients determined in this study

		CBZ	Phe
HO˙ reaction second order rate constant (M^{-1} s^{-1})	Free pollutant – previous studies	3.1 to 18 × 10^9 (ref. 65 and 66)	1.24 to 2.3 × 10^{10} (ref. 71 and 72)
	Free pollutant without surfactants – this study[a]	$(7.39 \pm 0.24) \times 10^{9a}$	$(1.22 \pm 0.16) \times 10^{10a}$
	Free pollutant with SDS below CMC – this study	$(7.25 \pm 0.54) \times 10^9$	$(1.31 \pm 0.20) \times 10^{11b}$
	Free pollutant with RLs below CMC – this study	$(6.86 \pm 0.24) \times 10^9$	$(1.13 \pm 0.23) \times 10^{10c}$
	Pollutant trapped in SDS micelles – this study	$(1.88 \pm 0.42) \times 10^9$	$(4.17 \pm 0.40) \times 10^{10b}$
	Pollutant trapped in RLs micelles – this study	$(2.67 \pm 0.42) \times 10^9$	nd[d]
K_{ow} (log K_{ow}) – previous studies		32–589 (1.51–2.77)[47–49]	2.88×10^4 to 4.47×10^4 (4.46–4.65)[50,51]
$K_{mw(SDS)}$ (log $K_{mw(SDS)}$) – this study		489 ± 171 (2.69)	$(1.1 \pm 10.9) \times 10^5$ (5.06)
$K_{mw(RLs)}$ (log $K_{mw(RLs)}$) – this study		2037 ± 1162 (3.31)	nd[d]

[a] Determined in ultrapure water at pH 8.2 adjusted with the 1 M KOH solution. [b] These values involve side processes, see text for details. [c] This value represents the arithmetic mean of all measurements obtained below the RLs' CMC in the series of experiments presented in SI-Fig. S1 with the corresponding standard deviation. [d] not determined.

existence of specific side processes resulting from the simultaneous presence of both Phe and SDS, as discussed in Section 3.4.

Fig. 2(b) shows that above the CMC, as with CBZ, the apparent reaction rate constant of Phe decreases. Fig. 4(a) shows the plot of the apparent reaction rate constant values as a function of total SDS micelle volume in the SDS concentration range of 2000–7000 mg L^{-1}, fitted with eqn (2). The resulting estimated values of the three equation parameters $k_{(w–Phe,HO^\bullet)}$, $k_{(SDSm–Phe,HO^\bullet)}$ and $K_{mw(Phe,SDS)}$ were $(1.31 \pm 0.20) \times 10^{11}$ M^{-1} s^{-1}, $(4.17 \pm 0.40) \times 10^{10}$ M^{-1} s^{-1} and $(1.1 \pm 10.9) \times 10^{5}$, respectively (Table 1). The $k_{(w–Phe,HO^\bullet)}$ value is irrelevant as it corresponds to the apparent reaction rate constant for water solubilized Phe at SDS concentration just below the CMC, thus including side degradation processes (discussed in Section 3.4). This fit also suffers from a large uncertainty in the $K_{SDSm–w,Phe}$ value, probably due to a lack of data in the 0–0.9 range for the mole fraction of Phe trapped in SDS micelles (Fig. 4(b)), making it statistically insignificant. Nevertheless, the corresponding estimated log $K_{mw(Phe,SDS)}$ value, 5.06, is only slightly above the log K_{ow} values of Phe reported in the literature, which range from 4.46 to 4.65.[50,51] The decrease in the apparent reaction rate constant observed above the CMC of SDS is consistent with the results obtained for CBZ, i.e. with a shielding effect of micelle

trapping. The estimated value of the second-order rate constant for the reaction of hydroxyl radicals with Phe molecules trapped in SDS micelles, $(4.17 \pm 0.40) \times 10^{10}$ M^{-1} s^{-1}, corresponds to a 68% decrease compared to the pre-CMC value. It is thus of the same order as that observed for CBZ (74%). Nevertheless, this $k_{(SDSm–Phe,HO^\bullet)}$ value remains significantly higher than the reaction rate constant obtained without any surfactant addition $((1.22 \pm 0.16) \times 10^{10}$ M^{-1} s$^{-1})$. This suggests that, although micelle trapping effectively protects Phe from the hydroxyl radical attack, it does not fully offset the increase in reactivity induced by free SDS monomers and does not significantly affect the degradation processes occurring along with the hydroxyl radical attack.

3.3. Degradation kinetics of CBZ in the presence of RLs

Fig. 5 shows the evolution of the experimental values of the apparent second-order rate constant of the reaction of CBZ with hydroxyl radicals in the presence of RLs. The general trend appears to be quite similar to that obtained with SDS, with a significant decrease in the apparent reaction rate constant at RL concentrations above the CMC. For RLs concentrations below the CMC, the rate constant value determined in the absence of RLs $((7.39 \pm 0.24) \times 10^{9}$ M^{-1} s$^{-1})$ is higher than the values obtained at 10 and 80 mg L^{-1} RLs $((6.77 \pm 0.26) \times 10^{9}$ M^{-1} s^{-1} and $(6.80 \pm 0.16) \times 10^{9}$ M^{-1} s^{-1} respectively), although the latter two values are not significantly different. While SDS clearly acts only as a quencher of hydroxyl radicals in the pre-micellar region, these results could suggest interactions of RLs with CBZ under similar conditions. Another explanation could be that RLs start forming aggregates at concentrations below the determined CMC, which was established by surface tension measurements. In any case, the dataset is too small to support any firm conclusion and the effect remains very limited compared to the decrease in the rate constant above the CMC. In this post-micellar region, CBZ behaves similarly to it behaviour with SDS, partitioning into micelles with corresponding
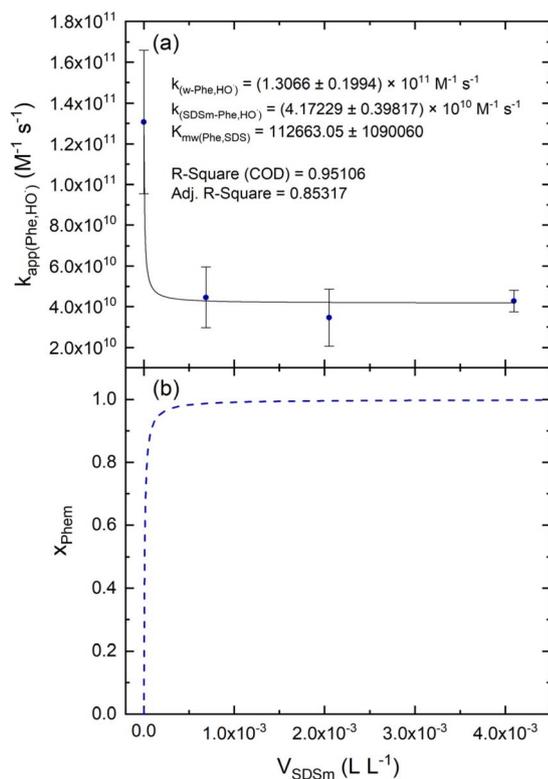

Fig. 4 (a) Apparent second-order reaction rate constant measured for the reaction of hydroxyl radicals with Phe as a function of estimated total SDS micelle volume fitted with eqn (2), for SDS concentrations in the range of 2000–7000 mg L^{-1}. (b) Corresponding estimated molar fraction of Phe trapped into SDS micelles as a function of estimated total SDS micelle volume.
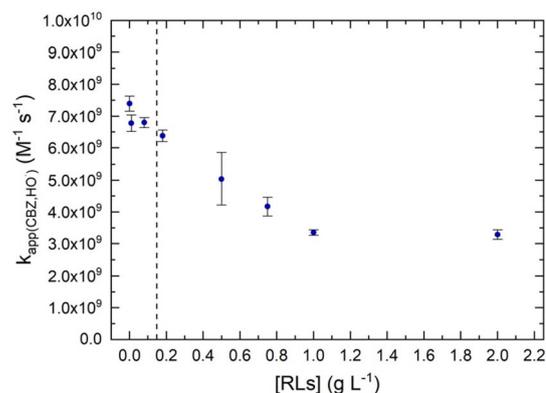

Fig. 5 Apparent second-order rate constant for the reaction of hydroxyl radicals with CBZ as a function of RL concentration. Error bars correspond to the uncertainty estimated based on the standard deviation of replicate measurements and the uncertainty associated with the $k_{(TPA,HO^\bullet)}$ value. The vertical dashed line indicates the CMC of RLs.

This journal is © The Royal Society of Chemistry 2025

Environ. Sci.: Processes Impacts, 2025, **27**, 3119–3131 | **3125**

shielding effects. At pH 8.2, RLs exist in their deprotonated form (pK_a ranging from 4.28 to 5.50 depending on concentration[74]) and are assumed to form micelles only, with negligible formation of larger structures such as of lamellae or vesicles.[75,76] The total volume of RL micelles, V_{RLsm}, was approximated using an estimated mean molecular weight of 577 g mol^{-1}, a micellar radius of 2.4 nm and a number of 25 monomers per micelle (ref. 15 and 76) (see the SI for details). The total volume of RL micelles, V_{RLsm}, increases linearly with RL concentration above the CMC (SI-Fig. S9(b)). The experimental values of $k_{app(CBZ,HO^\bullet)}$ were plotted as a function of V_{RLsm} and fitted using eqn (2) (Fig. 6(a)). The resulting estimated values of the three equation parameters $k_{(w-CBZ,HO^\bullet)}$, $k_{(RLsm-CBZ,HO^\bullet)}$ and $K_{mw(CBZ,RLs)}$ were $(6.86 \pm 0.24) \times 10^9$ M^{-1} s^{-1}, $(2.67 \pm 0.42) \times 10^9$ M^{-1} s^{-1} and 2037 ± 1162, respectively (Table 1). CBZ shielding by RL micelles thus results in a 61% decrease in the second-order rate constant of its reaction with hydroxyl radicals. It is interesting to note that the rate constant values obtained for CBZ trapped in micelles of SDS and RLs are not significantly different. The estimated value of log $K_{mw(CBZ,RLs)}$ is 3.31, with an uncertainty range of 2.94 to 3.51. This value is slightly higher than both the value obtained for SDS micelles and the log K_{ow} of CBZ (2.69 and 1.51–2.77 (ref. 47–49) respectively). This may indicate a higher propensity of RL micelles to trap CBZ compared to SDS micelles. Using this log $K_{mw(CBZ,RLs)}$ value, the molar fraction

of CBZ trapped in RL micelles was plotted as a function of RL concentration (Fig. 6(b)). As with SDS, the molar fraction of CBZ molecules trapped in RL micelles rapidly becomes non-negligible as the concentration of RLs increases. It should be pointed out that the value determined here as the CMC of RLs (145 mg L^{-1}) is similar to those obtained in most studies,[15,63] but has previously been shown to actually represent the critical aggregation concentration (CAC) above which only premicellar aggregates are formed, the true CMC occurring at a higher RL concentration (7.5 mM for monorhamnolipids, equivalent to 3.8 g L^{-1}).[76] Molecular dynamic simulations performed in this CAC–CMC range by Eismin et al.[76] predict loosely packed pre-micelles into which water can significantly penetrate. This suggests that fully formed RL micelles could have a higher shielding effect than the one quantified here. Nevertheless, our value seems relevant under environmental conditions with surfactant concentrations just above CMC.

3.4. Discussion

3.4.1. Influence of surfactants below the CMC. The presence of SDS or RL concentrations below the CMC induces no significant modification in the second-order rate constant of the reaction of hydroxyl radicals with the two model pollutants chosen, CBZ or Phe, except in the case of Phe in the presence of SDS. This suggests that, in many cases, solubilized surfactant monomers can reduce the half-life of organic pollutants relative to $^\bullet$OH reactions by acting solely as $^\bullet$OH radical quenchers. This effect alone can have a dramatic influence on the half-life of pollutants in organic-rich environments.[10] However, the notable ~11-fold increase in the apparent second-order rate constant of the reaction of Phe with increasing SDS concentrations below the CMC suggests that the situation can sometimes be more complex, requiring consideration of side processes. Here, the hypothesis that additional reactive species are produced during SDS degradation must be considered. Degradation of SDS molecules initiated by hydroxyl radicals has been shown to lead to the formation of peroxy (ROO$^\bullet$) and sulfate (SO$_4^{-\bullet}$) radicals,[77] both being able to react with organics. Given the second-order rate constant values determined in this study for the reaction of hydroxyl radicals with CBZ and Phe and those from previous studies for the reaction of sulfate radicals with TPA, CBZ and Phe, the expected $k_{HO^\bullet}/k_{SO_4^{-\bullet}}$ ratio (SI-Table S7) is only slightly higher for Phe than for CBZ (ratios ranging from 4 to 9 and from 3 to 4, respectively), while it is significantly higher for TPA (ratio of 26).[65,78–81] Compared to TPA, both CBZ and Phe should therefore appear affected by the formation of sulfate radicals, albeit to a slightly lesser extent in the case of CBZ. The fact that the reaction rate constant for CBZ appears unaffected by the hypothetic formation of sulfate radicals, suggests that additional side processes contribute to the increasing rate constants observed for Phe with SDS concentration.

3.4.2. Influence of surfactants above the CMC. Above the CMC, a similar trend is observed in the evolution of the apparent second-order rate constant for the three experimental conditions tested. The partitioning of the pollutant in the micelles of surfactants decreases its apparent reaction rate
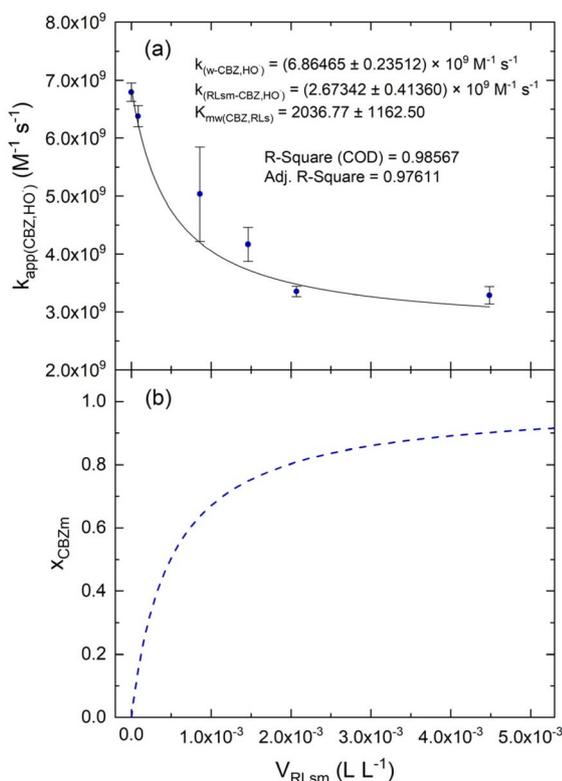

Fig. 6 (a) Apparent second-order reaction rate constant measured for the reaction of hydroxyl radicals with CBZ as a function of estimated total RL micelle volume fitted with eqn (2). (b) Corresponding estimated molar fraction of CBZ trapped into RL micelles as a function of estimated total RL micelle volume.

3126 | *Environ. Sci.: Processes Impacts*, 2025, **27**, 3119–3131

This journal is © The Royal Society of Chemistry 2025

constant with hydroxyl radicals, according to previous studies.[82,83] Here, the results show that this decrease reaches a plateau when the micellar volume becomes sufficient to trap all the available pollutant molecules. Interestingly, the magnitude of this decrease is quite similar for both model pollutants and model surfactants, with a reduction by a factor of about 3 (3.9, 3.1 and 2.6 for CBZ with SDS, Phe with SDS and CBZ with RLs respectively). A similar extent was reported by Bansal *et al.*[83] for the degradation of benzene initiated by H_2O_2 photolysis in solutions of three different surfactants, with second-order reaction rate constants with hydroxyl radicals decreasing from 8.2 to $2.6–3.0 \times 10^9$ M^{-1} s^{-1}. SDS has also been shown by Faust and Abbatt[84] to slow down the rate of the heterogeneous reactions involving a highly hydrophilic compound (tricarballylic acid) solubilized in aqueous droplets with gas phase hydroxyl radicals. Despite the heterogeneous nature of the chemistry involved in this case, the observed decrease in the reaction rate fell within the same order of magnitude, with a decrease of about 60% in the presence of a SDS monolayer at the water surface.[84] The consistency of all these results provides an interesting starting point for considering such modified kinetics in the assessment of the fate of organic pollutants in surfactant-rich environments.

In addition, the results presented here indicate that the commonly available K_{ow} value could be employed to assess the molar fraction of a pollutant that partitions into a given volume of micelles, even for relatively water-soluble compounds. A limitation may be the required absence of ionic or other interactions between the hydrophilic head group of the surfactant and the pollutant, as it was the case in this study with nonionic pollutants and anionic surfactants. For hydrophobic compounds, some K_{ow}–K_{mw} relationships can be found in the literature.[16,85]

These findings may also be used as a preliminary indication of how reaction kinetics may be modified in other surfactant-organized structures, including surfactant mono- or multi-layers at water–air interfaces (*e.g.* SML or atmospheric droplets) and vesicles and lamellae for media with higher surfactant concentrations.

4. Conclusion

This study focused on the determination of the kinetics of the reaction of the hydroxyl radical with pollutants in surfactant rich media. It was shown that, in the absence of side processes, the presence of monomers of the two tested surfactants, SDS (a well-known anionic surfactant) and RLs (a biogenic surfactant), at concentrations below the CMC does not significantly affect the value of the second-order reaction rate constant. In these concentration ranges, the pollutant degradation can nevertheless be slowed down by the quenching of hydroxyl radicals by the surfactant monomers. In some cases, side processes can also occur and affect the degradation kinetics at sub-CMC concentrations. Here, SDS degradation was for instance suspected to produce additional reactive species capable of accelerating the degradation kinetics of Phe. Above the CMC, partitioning of the pollutant into surfactant micelles induces

a decrease in the reaction rate constant, shielding it from the hydroxyl radical attack. Values of these second-order reaction rate constants were determined for pollutant molecules trapped into micelles and shown to be a factor of about three times lower compared to those obtained under premicellar conditions, in good agreement with previous studies. The estimated K_{mw} values were in good agreement with K_{ow} values for both tested pollutants, with little impact from the surfactant type in the case of CBZ.

Organic pollutants are known to be enriched in surfactant-rich environments such as the SML, atmospheric aerosols, fog droplets and even evaporative waters. This work appears to provide a suitable foundation for evaluating the impact of such surfactant-rich environments on the half-life and fate of these pollutants and an interesting indication of how reaction kinetics may be modified in various organized surfactant structures. Future studies may explore the influence of surfactants on direct photolysis and degradation processes initiated by other reactive species, such as the triplet state of organic matter or singlet oxygen. Another emerging question is whether the reaction pathways and the structure of the degradation products formed in these environments are modified.

Conflicts of interest

There are no conflicts to declare.

Data availability

Raw data files can be obtained by contacting the corresponding author.

The Supplementary Information provides details on the experimental procedures and data processing, as well as complementary experimental results. See DOI: **https://doi.org/10.1039/d5em00203f**.

Acknowledgements

References

1 J. Socorro, A. Durand, B. Temime-Roussel, S. Gligorovski, H. Wortham and E. Quivet, The persistence of pesticides in atmospheric particulate phase: an emerging air quality issue, *Sci. Rep.*, 2016, **6**, 33456, DOI: **10.1038/srep33456**.

2 J. Socorro, P. S. J. Lakey, L. Han, T. Berkemeier, G. Lammel, C. Zetzsch, U. Pöschl and M. Shiraiwa, Heterogeneous OH oxidation, shielding effects, and implications for the atmospheric fate of terbuthylazine and other pesticides, *Environ. Sci. Technol.*, 2017, **51**, 13749–13754, DOI: **10.1021/acs.est.7b04307**.

3 M. Shrivastava, S. Lou, A. Zelenyuk, R. C. Easter, R. A. Corley, B. D. Thrall, P. J. Rasch, J. D. Fast, S. L. Massey Simonich, H. Shen and S. Tao, Global long-range transport and lung

This journal is © The Royal Society of Chemistry 2025

Environ. Sci.: Processes Impacts, 2025, **27**, 3119–3131 | **3127**

cancer risk from polycyclic aromatic hydrocarbons shielded by coatings of organic aerosol, *Proc. Natl. Acad. Sci. U. S. A.*, 2017, **114**, 1246–1251, DOI: **10.1073/pnas.1618475114**.

4 C. Mattei, H. Wortham and E. Quivet, Heterogeneous atmospheric degradation of pesticides by ozone: influence of relative humidity and particle type, *Sci. Total Environ.*, 2018, **625**, 1544–1553, DOI: **10.1016/j.scitotenv.2018.01.049**.

5 B. T. Mmereki, D. J. Donaldson, J. B. Gilman, T. L. Eliason and V. Vaida, Kinetics and products of the reaction of gas-phase ozone with anthracene adsorbed at the air–aqueous interface, *Atmos. Environ.*, 2004, **38**, 6091–6103, DOI: **10.1016/j.atmosenv.2004.08.014**.

6 E. A. Henderson and D. J. Donaldson, Influence of organic coatings on pyrene ozonolysis at the air–aqueous interface, *J. Phys. Chem. A*, 2012, **116**, 423–429, DOI: **10.1021/jp2094627**.

7 C. Zhou, J. Chen, H. Xie, Y. Zhang, Y. Li, Y. Wang, Q. Xie and S. Zhang, Modeling photodegradation kinetics of organic micropollutants in water bodies: a case of the Yellow River estuary, *J. Hazard. Mater.*, 2018, **349**, 60–67, DOI: **10.1016/j.jhazmat.2018.01.051**.

8 M. Bodrato and D. Vione, APEX (Aqueous Photochemistry of Environmentally occurring Xenobiotics): a free software tool to predict the kinetics of photochemical processes in surface waters, *Environ. Sci.: Processes Impacts*, 2014, **16**, 732–740, DOI: **10.1039/C3EM00541K**.

9 L. S. Albi, Z. Guo, G. Chen and C. Yoshimura, Potential effect of atmospheric condition on incident light and photo-production of reactive intermediates in freshwater systems, *Environ. Adv.*, 2023, **11**, 100346, DOI: **10.1016/j.envadv.2023.100346**.

10 A. Rosso and D. Vione, Pollutant photodegradation affected by evaporative water concentration in a climate change scenario, *Molecules*, 2024, **29**, 2655, DOI: **10.3390/molecules29112655**.

11 J. W. Park and P. R. Jaffe, Partitioning of three nonionic organic compounds between adsorbed surfactants, micelles, and water, *Environ. Sci. Technol.*, 1993, **27**, 2559–2565, DOI: **10.1021/es00048a038**.

12 J. C. Mata-Sandoval, J. Karns and A. Torrents, Effect of rhamnolipids produced by pseudomonas aeruginosa UG2 on the solubilization of pesticides, *Environ. Sci. Technol.*, 2000, **34**, 4923–4930, DOI: **10.1021/es0011111**.

13 C. N. Mulligan, Environmental applications for biosurfactants, *Environ. Pollut.*, 2005, **133**, 183–198, DOI: **10.1016/j.envpol.2004.06.009**.

14 J. A. Marqusee and K. A. Dill, Solute partitioning into chain molecule interphases: monolayers, bilayer membranes, and micelles, *J. Chem. Phys.*, 1986, **85**, 434–444, DOI: **10.1063/1.451621**.

15 V. P. Arkhipov, R. V. Arkhipov, E. V. Petrova and A. Filippov, Micellar and solubilizing properties of rhamnolipids, *Magn. Reson. Chem.*, 2023, **61**, 345–355, DOI: **10.1002/mrc.5337**.

16 K. T. Valsaraj and L. J. Thibodeaux, Relationships between micelle-water and octanol-water partition constants for hydrophobic organics of environmental interest, *Water Res.*, 1989, **23**, 183–189, DOI: **10.1016/0043-1354(89)90042-0**.

17 L. Zhu and S. Feng, Synergistic solubilization of polycyclic aromatic hydrocarbons by mixed anionic–nonionic surfactants, *Chemosphere*, 2003, **53**, 459–467, DOI: **10.1016/S0045-6535(03)00541-1**.

18 B. Samiey, C.-H. Cheng and J. Wu, Effects of surfactants on the rate of chemical reactions, *J. Chem.*, **2014**, e908476, DOI: **10.1155/2014/908476**.

19 G. La Sorella, G. Strukul and A. Scarso, Recent advances in catalysis in micellar media, *Green Chem.*, 2015, **17**, 644–683, DOI: **10.1039/C4GC01368A**.

20 D. Yordanova, E. Ritter, T. Gerlach, J. H. Jensen, I. Smirnova and S. Jakobtorweihen, Solute partitioning in micelles: combining molecular dynamics simulations, COSMOmic, and experiments, *J. Phys. Chem. B*, 2017, **121**, 5794–5809, DOI: **10.1021/acs.jpcb.7b03147**.

21 S. M. Thomas and S. K. Harrison, Surfactant-altered rates of chlorimuron and metsulfuron photolysis in sunlight, *Weed Sci.*, 1990, **38**, 602–606, DOI: **10.1017/S0043174500051560**.

22 K. Kalyanasundaram, *Photochemistry in microheterogeneous systems*, Elsevier, 2012.

23 C. A. Bunton and G. Savelli, Organic reactivity in aqueous micelles and similar assemblies, in *Advances in physical organic chemistry*, ed. V. Gold and D. Bethell, Academic Press, 1986, vol. 22, pp. 213–309, DOI: **10.1016/S0065-3160(08)60169-0**.

24 O. Wurl, E. Wurl, L. Miller, K. Johnson and S. Vagle, Formation and global distribution of sea-surface microlayers, *Biogeosciences*, 2011, **8**, 121–135, DOI: **10.5194/bg-8-121-2011**.

25 B. Sabbaghzadeh, R. C. Upstill-Goddard, R. Beale, R. Pereira and P. D. Nightingale, The Atlantic Ocean surface microlayer from 50°N to 50°S is ubiquitously enriched in surfactants at wind speeds up to 13 m s⁻¹, *Geophys. Res. Lett.*, 2017, **44**, 2017GL072988, DOI: **10.1002/2017GL072988**.

26 B. Ćosović, Surface-active properties of the sea surface microlayer and consequences for pollution in the Mediterranean Sea, in *The Mediterranean Sea. Handbook of environmental chemistry*, ed. Saliot A., Springer, Berlin, Heidelberg, 2005, vol. 5K, pp. 269–296.

27 O. Wurl, L. Miller, R. Röttgers and S. Vagle, The distribution and fate of surface-active substances in the sea-surface microlayer and water column, *Mar. Chem.*, 2009, **115**, 1–9, DOI: **10.1016/j.marchem.2009.04.007**.

28 M. Cunliffe, A. Engel, S. Frka, B. Gašparović, C. Guitart, J. C. Murrell, M. Salter, C. Stolle, R. Upstill-Goddard and O. Wurl, Sea surface microlayers: a unified physicochemical and biological perspective of the air–ocean interface, *Prog. Oceanogr.*, 2013, **109**, 104–116, DOI: **10.1016/j.pocean.2012.08.004**.

29 P. Schmitt-Kopplin, G. Liger-Belair, B. P. Koch, R. Flerus, G. Kattner, M. Harir, B. Kanawati, M. Lucio, D. Tziotis, N. Hertkorn and I. Gebefügi, Dissolved organic matter in sea spray: a transfer study from marine surface water to aerosols, *Biogeosciences*, 2012, **9**, 1571–1582, DOI: **10.5194/bg-9-1571-2012**.

30 Y. Song, J. Li, N. T. Tsona, L. Liu and L. Du, Enrichment of short-chain organic acids transferred to submicron sea

3128 | *Environ. Sci.: Processes Impacts*, 2025, **27**, 3119–3131

This journal is © The Royal Society of Chemistry 2025

spray aerosols, *Sci. Total Environ.*, 2022, **851**, 158122, DOI: 10.1016/j.scitotenv.2022.158122.

31 N. Radoman, Enrichment of biogenic and anthropogenic organic substances on sea spray aerosols, PhD thesis, Department of Materials and Environmental Chemistry, Stockholm University, 2022, ISBN: 978-91-8014-097-3.

32 G. de Leeuw, E. L. Andreas, M. D. Anguelova, C. W. Fairall, E. R. Lewis, C. O'Dowd, M. Schulz and S. E. Schwartz, Production flux of sea spray aerosol, *Rev. Geophys.*, 2011, **49**(2), RG2001, DOI: 10.1029/2010RG000349.

33 C. Guigue, M. Tedetti, S. Giorgi and M. Goutx, Occurrence and distribution of hydrocarbons in the surface microlayer and subsurface water from the urban coastal marine area off Marseilles, Northwestern Mediterranean Sea, *Mar. Pollut. Bull.*, 2011, **62**, 2741–2752, DOI: 10.1016/j.marpolbul.2011.09.013.

34 O. Wurl and J. P. Obbard, A review of pollutants in the sea-surface microlayer (SML): a unique habitat for marine organisms, *Mar. Pollut. Bull.*, 2004, **48**, 1016–1030, DOI: 10.1016/j.marpolbul.2004.03.016.

35 A. Cincinelli, A. M. Stortini, L. Checchini, T. Martellini, M. D. Bubba and L. Lepri, Enrichment of organic pollutants in the sea surface microlayer (SML) at Terra Nova Bay, Antarctica: influence of SML on superficial snow composition, *J. Environ. Monit.*, 2005, **7**, 1305–1312, DOI: 10.1039/B507321A.

36 C. Guitart, N. García-Flor, J. C. Miquel, S. W. Fowler and J. Albaigés, Effect of the accumulation of polycyclic aromatic hydrocarbons in the sea surface microlayer on their coastal air–sea exchanges, *J. Mar. Syst.*, 2010, **79**, 210–217, DOI: 10.1016/j.jmarsys.2009.09.003.

37 G. Casas, A. Martínez-Varela, J. L. Roscales, M. Vila-Costa, J. Dachs and B. Jiménez, Enrichment of perfluoroalkyl substances in the sea-surface microlayer and sea-spray aerosols in the Southern Ocean, *Environ. Pollut.*, 2020, **267**, 115512, DOI: 10.1016/j.envpol.2020.115512.

38 A. Cincinelli, A. M. Stortini, M. Perugini, L. Checchini and L. Lepri, Organic pollutants in sea-surface microlayer and aerosol in the coastal environment of Leghorn—(Tyrrhenian Sea), *Mar. Chem.*, 2001, **76**, 77–98, DOI: 10.1016/S0304-4203(01)00049-4.

39 R. Uning, M. T. Latif, K. L. Yu, S. Y. Cheng, F. Ahamad, M. F. Khan, E. A. Bedurus and S. Suratman, Surfactants in the sea surface microlayer, underlying ater and atmospheric particles of tropical coastal ecosystems, *Water, Air, Soil Pollut.*, 2018, **229**, 305, DOI: 10.1007/s11270-018-3961-4.

40 S. Shaharom, M. T. Latif, M. F. Khan, S. N. M. Yusof, N. A. Sulong, N. B. A. Wahid, R. Uning and S. Suratman, Surfactants in the sea surface microlayer, subsurface water and fine marine aerosols in different background coastal areas, *Environ. Sci. Pollut. Res.*, 2018, **25**, 27074–27089, DOI: 10.1007/s11356-018-2745-0.

41 F. Pawlak, K. Koziol, M. Frankowski, Ł. Nowicki, C. Marlin, A. M. Sulej-Suchomska and Ż. Polkowska, Sea spray as a secondary source of chlorinated persistent organic pollutants? – Conclusions from a comparison of seven fresh snowfall events in 2019 and 2021, *Sci. Total Environ.*, 2023, **891**, 164357, DOI: 10.1016/j.scitotenv.2023.164357.

42 J. H. Johansson, M. E. Salter, J. C. A. Navarro, C. Leck, E. D. Nilsson and I. T. Cousins, Global transport of perfluoroalkyl acids via sea spray aerosol, *Environ. Sci.: Processes Impacts*, 2019, **21**, 635–649, DOI: 10.1039/C8EM00525G.

43 B. T. Mmereki and D. J. Donaldson, Laser induced fluorescence of pyrene at an organic coated air–water interface, *Phys. Chem. Chem. Phys.*, 2002, **4**, 4186–4191, DOI: 10.1039/B204754C.

44 B. T. Mmereki, S. R. Chaudhuri and D. J. Donaldson, Enhanced uptake of PAHs by organic-coated aqueous surfaces, *J. Phys. Chem. A*, 2003, **107**, 2264–2269, DOI: 10.1021/jp027361g.

45 E. M. McLay, C. A. Nour, Y. Y. Huang, Z. M. Golay, P. Wong-Wah-Chung, S. Rossignol and D. J. Donaldson, Experimental determination of the partitioning of representative organic pollutants to the air–water interface, *Environ. Sci.: Processes Impacts*, 2024, **26**, 510–518, DOI: 10.1039/D3EM00394A.

46 Y.-J. An and E. R. Carraway, PAH degradation by UV/H$_2$O$_2$ in perfluorinated surfactant solutions, *Water Res.*, 2002, **36**, 309–314, DOI: 10.1016/S0043-1354(01)00206-8.

47 T. Scheytt, P. Mersmann, R. Lindstädt and T. Heberer, 1-Octanol/water partition coefficients of 5 pharmaceuticals from human medical care: carbamazepine, clofibric acid, diclofenac, ibuprofen, and propyphenazone, *Water, Air, Soil Pollut.*, 2005, **165**, 3–11, DOI: 10.1007/s11270-005-3539-9.

48 A. Pyca, M. Babuska and M. Zachariasz, A comparison of theoretical methods of calculation of partition coefficients for selected drugs, *Acta Pol. Pharm.*, 2006, **63**, 159–167.

49 S. Lee, S.-I. Kang, J.-L. Lim, Y. J. Huh, K.-S. Kim and J. Cho, Evaluating controllability of pharmaceuticals and metabolites in biologically engineered processes, using corresponding octanol–water distribution coefficient, *Ecol. Eng.*, 2011, **37**, 1595–1600, DOI: 10.1016/j.ecoleng.2011.04.007.

50 P. G.-J. de Maagd, D. T. E. M. ten Hulscher, H. van den Heuvel, A. Opperhuizen and D. T. H. M. Sijm, Physicochemical properties of polycyclic aromatic hydrocarbons: aqueous solubilities, *n*-octanol/water partition coefficients, and Henry's law constants, *Environ. Toxicol. Chem.*, 1998, **17**, 251–257, DOI: 10.1002/etc.5620170216.

51 F. Alves de Lima Ribeiro and M. M. C. Ferreira, QSPR models of boiling point, octanol–water partition coefficient and retention time index of polycyclic aromatic hydrocarbons, *J. Mol. Struct.: THEOCHEM*, 2003, **663**, 109–126, DOI: 10.1016/j.theochem.2003.08.107.

52 A. Monod, L. Poulain, S. Grubert, D. Voisin and H. Wortham, Kinetics of OH-initiated oxidation of oxygenated organic compounds in the aqueous phase: new rate constants, structure–activity relationships and atmospheric implications, *Atmos. Environ.*, 2005, **39**, 7667–7688, DOI: 10.1016/j.atmosenv.2005.03.019.

This journal is © The Royal Society of Chemistry 2025

Environ. Sci.: Processes Impacts, 2025, **27**, 3119–3131 | 3129

53 T. Charbouillot, M. Brigante, G. Mailhot, P. R. Maddigapu, C. Minero and D. Vione, Performance and selectivity of the terephthalic acid probe for OH as a function of temperature, pH and composition of atmospherically relevant aqueous media, *J. Photochem. Photobiol., A*, 2011, **222**, 70–76, DOI: **10.1016/j.jphotochem.2011.05.003**.

54 S. Page, W. Arnold and K. McNeill, Terephthalate as a probe for photochemically generated hydroxyl radical, *J. Environ. Monit.*, 2010, **12**, 1658–1665, DOI: **10.1039/C0EM00160K**.

55 A. Cid, A. Acuña, M. Alonso-Ferrer, G. Astray, L. García-Río, J. Simal-Gándara, J. C. Mejuto, Pseudophase model in microemulsions, In: Microemulsion – a Chemical Nanoreactor, IntechOpen, 2019, 978-1-78984-544-0.

56 F. M. Menger and C. E. Portnoy, Chemistry of reactions proceeding inside molecular aggregates, *J. Am. Chem. Soc.*, 1967, **89**, 4698–4703, DOI: **10.1021/ja00994a023**.

57 M. Pérez-Rodríguez, G. Prieto, C. Rega, L. M. Varela, F. Sarmiento and V. Mosquera, A Comparative Study of the Determination of the Critical Micelle Concentration by Conductivity and Dielectric Constant Measurements, *Langmuir*, 1998, **14**, 4422–4426, DOI: **10.1021/la980296a**.

58 I. M. Umlong and K. Ismail, Micellization behaviour of sodium dodecyl sulfate in different electrolyte media, *Colloids Surf., A*, 2007, **299**, 8–14, DOI: **10.1016/j.colsurfa.2006.11.010**.

59 G. Basu Ray, I. Chakraborty and S. P. Moulik, Pyrene absorption can be a convenient method for probing critical micellar concentration (cmc) and indexing micellar polarity, *J. Colloid Interface Sci.*, 2006, **294**, 248–254, DOI: **10.1016/j.jcis.2005.07.006**.

60 M. Layek, S. Kundu, P. Karmakar, S. M. Rahaman, T. Mandal, A. Patra, A. Nandy, M. Chakravarty, P. Sar and B. Saha, Optimizing homologous alcohol oxidation: elucidating the impact of surfactant-alcohol hydrophobic interaction and micellar surface charge, *Res. Chem. Intermed.*, 2025, **51**, 311–330, DOI: **10.1007/s11164-024-05461-9**.

61 Z. Li, Y. Zhang, J. Lin, W. Wang and S. Li, High-yield di-rhamnolipid production by pseudomonas aeruginosa YM4 and its potential application in MEOR, *Molecules*, 2019, **24**, 1433, DOI: **10.3390/molecules24071433**.

62 Y. Zhang, T. L. Placek, R. Jahan, P. Alexandridis and M. Tsianou, Rhamnolipid micellization and adsorption properties, *Int. J. Mol. Sci.*, 2022, **23**, 11090, DOI: **10.3390/ijms231911090**.

63 I. E. Kłosowska-Chomiczewska, K. Mędrzycka, E. Hallmann, E. Karpenko, T. Pokynbroda, A. Macierzanka and C. Jungnickel, Rhamnolipid CMC prediction, *J. Colloid Interface Sci.*, 2017, **488**, 10–19, DOI: **10.1016/j.jcis.2016.10.055**.

64 G. V. Buxton, C. L. Greenstock, W. P. Helman and A. B. Ross, Critical review of rate constants for reactions of hydrated electrons, hydrogen atoms and hydroxyl radicals ($^\bullet$OH/$^\bullet$O$^-$) in aqueous solution, *J. Phys. Chem. Ref. Data*, 1988, **17**, 513–886, DOI: **10.1063/1.555805**.

65 R. Xiao, J. Ma, Z. Luo, W. Zeng, Z. Wei, R. Spinney, W. Hu and D. D. Dionysiou, Experimental and theoretical insight into hydroxyl and sulfate radicals-mediated degradation of carbamazepine, *Environ. Pollut.*, 2020, **257**, 113498, DOI: **10.1016/j.envpol.2019.113498**.

66 E. De Laurentiis, S. Chiron, S. Kouras-Hadef, C. Richard, M. Minella, V. Maurino, C. Minero and D. Vione, Photochemical fate of carbamazepine in surface freshwaters: laboratory measures and modeling, *Environ. Sci. Technol.*, 2012, **46**, 8164–8173, DOI: **10.1021/es3015887**.

67 D. Vogna, R. Marotta, R. Andreozzi, A. Napolitano and M. d'Ischia, Kinetic and chemical assessment of the UV/H$_2$O$_2$ treatment of antiepileptic drug carbamazepine, *Chemosphere*, 2004, **54**, 497–505, DOI: **10.1016/S0045-6535(03)00757-4**.

68 M. Srabovic, M. Poljakovic and E. Pehlic, Micellar solubilization of carbamazepine, *J. Sci. Res. Rep.*, 2014, 3106–3116, DOI: **10.9734/JSRR/2014/12362**.

69 J. R. Crison, N. D. Weiner and G. L. Amidon, Dissolution media for in vitro testing of water-insoluble drugs: effect of surfactant purity and electrolyte on in vitro dissolution of carbamazepine in aqueous solutions of sodium lauryl sulfate, *J. Pharm. Sci.*, 1997, **86**, 384–388, DOI: **10.1021/js960105t**.

70 G. Duplâtre, M. F. Ferreira Marques and M. da Graça Miguel, Size of sodium dodecyl sulfate micelles in aqueous solutions as studied by positron annihilation lifetime spectroscopy, *J. Phys. Chem.*, 1996, **100**, 16608–16612, DOI: **10.1021/jp960644m**.

71 F. J. Beltrán, G. Ovejero and J. Rivas, Oxidation of polynuclear aromatic hydrocarbons in water. 3. UV radiation combined with hydrogen peroxide, *Ind. Eng. Chem. Res.*, 1996, **35**, 883–890, DOI: **10.1021/ie950363l**.

72 M. E. Lindsey and M. A. Tarr, Inhibited hydroxyl radical degradation of aromatic hydrocarbons in the presence of dissolved fulvic acid, *Water Res.*, 2000, **34**, 2385–2389, DOI: **10.1016/S0043-1354(99)00391-7**.

73 W. R. Haag and C. C. D. Yao, Rate constants for reaction of hydroxyl radicals with several drinking water contaminants, *Environ. Sci. Technol.*, 1992, **26**, 1005–1013, DOI: **10.1021/es00029a021**.

74 A. Lebrón-Paler, J. E. Pemberton, B. A. Becker, W. H. Otto, C. K. Larive and R. M. Maier, Determination of the acid dissociation constant of the biosurfactant monorhamnolipid in aqueous solution by potentiometric and spectroscopic methods, *Anal. Chem.*, 2006, **78**, 7649–7658, DOI: **10.1021/ac0608826**.

75 J. T. Champion, J. C. Gilkey, H. Lamparski, J. Retterer and R. M. Miller, Electron microscopy of rhamnolipid (biosurfactant) morphology: effects of pH, cadmium, and octadecane, *J. Colloid Interface Sci.*, 1995, **170**, 569–574, DOI: **10.1006/jcis.1995.1136**.

76 R. J. Eismin, E. Munusamy, L. L. Kegel, D. E. Hogan, R. M. Maier, S. D. Schwartz and J. E. Pemberton, Evolution of aggregate structure in solutions of anionic monorhamnolipids: experimental and computational results, *Langmuir*, 2017, **33**, 7412–7424, DOI: **10.1021/acs.langmuir.7b00078**.

3130 | *Environ. Sci.: Processes Impacts*, 2025, **27**, 3119–3131

This journal is © The Royal Society of Chemistry 2025

77 S. I. M. Ng, K. H. Ng, P. W. F. Yeung, R. Xu, P.-K. So, Y. Huang, J. Z. Yu, C. K. K. Choi, Y.-L. S. Tse and M. N. Chan, Chemical transformation of a long-chain alkyl organosulfate via heterogeneous OH oxidation: a case study of sodium dodecyl sulfate, *Environ. Sci.: Atmos.*, 2022, **2**, 1060–1075, DOI: **10.1039/D2EA00026A**.

78 L. Wojnárovits and E. Takács, Rate constants of sulfate radical anion reactions with organic molecules: a review, *Chemosphere*, 2019, **220**, 1014–1032, DOI: **10.1016/j.chemosphere.2018.12.156**.

79 Y. Tao, O. Monfort, M. Brigante, H. Zhang and G. Mailhot, Phenanthrene decomposition in soil washing effluents using UVB activation of hydrogen peroxide and peroxydisulfate, *Chemosphere*, 2021, **263**, 127996, DOI: **10.1016/j.chemosphere.2020.127996**.

80 R. Matta, S. Tlili, S. Chiron and S. Barbati, Removal of carbamazepine from urban wastewater by sulfate radical oxidation, *Environ. Chem. Lett.*, 2011, **9**, 347–353, DOI: **10.1007/s10311-010-0285-z**.

81 P. Neta, V. Madhavan, H. Zemel and R. W. Fessenden, Rate constants and mechanism of reaction of sulfate radical anion with aromatic compounds, *J. Am. Chem. Soc.*, 1977, **99**, 163–164, DOI: **10.1021/ja00443a030**.

82 Y.-J. An and E. R. Carraway, PAH degradation by UV/H_2O_2 in perfluorinated surfactant solutions, *Water Res.*, 2002, **36**, 309–314, DOI: **10.1016/S0043-1354(01)00206-8**.

83 K. M. Bansal, L. K. Patterson, E. J. Fendler and J. H. Fendler, Reactions of hydrated electrons, hydrogen atoms and hydroxyl radicals in micellar systems, *Int. J. Radiat. Phys. Chem.*, 1971, **3**, 321–331, DOI: **10.1016/0020-7055(71)90033-7**.

84 J. A. Faust and J. P. D. Abbatt, Organic surfactants protect dissolved aerosol components against heterogeneous oxidation, *J. Phys. Chem. A*, 2019, **123**, 2114–2124, DOI: **10.1021/acs.jpca.9b00167**.

85 C. T. Jafvert, L. V. H. Patricia and J. K. Heath, Solubilization of non-polar compounds by non-ionic surfactant micelles, *Water Res.*, 1994, **28**, 1009–1017, DOI: **10.1016/0043-1354(94)90185-6**.

This journal is © The Royal Society of Chemistry 2025

Environ. Sci.: Processes Impacts, 2025, **27**, 3119–3131 | **3131**